Analysis of Thin-Walled Closed Beams With General Quadrilateral Cross Sections

J. H. Kim
Research Associate,
Institute of Advanced Machinery and Design

Y. Y. Kim
Associate Professor

School of Mechanical and
Aerospace Engineering,
Seoul National University,
Kwanak-Gu, Shinlim-Dong, San 56-1,
Seoul 151-742, Korea

This paper deals with the one-dimensional static and dynamic analysis of thin-walled closed beams with general quadrilateral cross sections. The coupled deformations of distortion as well as torsion and warping are investigated in this work. A new approach to determine the functions describing section deformations is proposed. In particular, the present distortion function satisfies all the necessary continuity conditions unlike Vlasov's distortion function. Based on these section deformation functions, a one-dimensional theory dealing with the coupled deformations is presented. The actual numerical work is carried out using two-node C^0 finite element formulation. The present one-dimensional results for some static and free-vibration problems are compared with the existing and the plate finite element results.

Introduction

Thin-walled closed beams are preferred over thin-walled open beams particularly when high torsional rigidities are required. However, it is difficult to predict their behavior accurately with simplified theories. The purpose of this paper is to analyze the static and dynamic coupled deformation of torsion, warping, and distortion of thin-walled closed beams with general quadrilateral cross sections using a one-dimensional beam theory. In particular, a function describing distortional deformation of the beam cross section is newly proposed to develop a one-dimensional theory. For the numerical analysis based on the one-dimensional beam theory, a two-node C^0 finite element formulation is performed.

Vlasov (1961) offered a most comprehensive theoretical analysis of thin-walled structures. Thereafter many papers have been published on thin-walled closed beams, and an excellent review on this subject is given in Maisel (1982). Křístek (1970) solves the problem of nonuniform torsion in tapered box beams and considers the effect force deforming the cross section. Cheung (1969) uses the finite strip method for folded plates and employs Fourier series for the expansion in the longitudinal direction. Jirousek et al. (1979) propose a macro-element, which consists of a modified Ahmad thick shell element and an assembly element.

Bažant and Nimeiri (1974) develop a skew-ended finite element for curved box beams, using a mapping process of a rectangular element with a square cross section. Considering distortion and warping, Boswell and Zhang (1983) present finite beam element formulation for the static analysis and later report some related experimental results (1985). Zhang and Lyons (1984a, 1984b) develop a multi-cell box beam finite element for the analysis of curved bridges, and Boswell and Li (1995) discuss warping functions due to torsion and distortion. Razzaqpur and Li (1991a, 1991b) consider warping and distortion deformations in the study of multi-cell box beams. They also extend their theory to the curved thin-walled box beams (1994). Mikkola and Paavola (1980) suggest a finite element method for elastic box beams. Paavola (1992) presents a discrete finite element method in which the cross sections are assumed to consist of piecewise rectilinear cross sections of separate shells. However, the focus of these papers is not on the accurate determination of the distortional shape function of thin-walled beams with general cross sections. The accurate distortional shape function, like other sectional deformation shape functions, is very important in obtaining accurate results particularly for vibration problems.

As far as the distortion shape function is concerned, Vlasov (1961) discusses the distortional shape for a rectangular box beam. Bažant and Nimeiri (1974) map the distortion shape of the rectangular box beam into that of the trapezoidal box beam. Boswell and Zhang (1984) deal with the distortion function of the box beams with one symmetry axis. Maisel (1982) also discusses distortional shapes for polygonal sectioned box beams on the assumption that the cross section can be viewed as a hinged system. However, it seems that these approaches are difficult to extend directly to beams with arbitrary cross sections including general quadrilateral cross sections. The consideration of the distortional deformation is generally more significant in dynamic analysis. For instance, the significance of sectional deformations, such as distortion, is addressed in the vibration analysis of a box-beam T-joint (Kim et al., 1995). Although several papers (Gere, 1954; Bishop et al., 1983; Friberg, 1985; Zhang and Chen, 1990; Kou et al., 1992; Kim et al., 1994a, b; Laudiero and Savoia, 1991) consider dynamic problems, these papers do not take into account both warping and distortion.

In the present paper we present a new method to determine warping and distortion functions for general quadrilateral cross-sectioned thin-walled beams. First we apply the virtual work concept to impose the orthogonality conditions of warping and distortional functions with respect to some sectional rigid-body motions, which physically correspond to extension, torsion, bending, and flexure. Although these conditions suffice for the determination of an approximate warping function, additional rotation/moment continuity conditions at the corners of the contour of the quadrilateral cross section need to be taken into account in the case of distortion functions. In finding a distortion function for rectangular cross sections, Vlasov (1961) sacrifices the displacement continuity at the corner in order to satisfy more important rotation/moment continuity conditions; the importance of the displacement continuity in rectangular cross-sectioned beam has been addressed in Kim and Kim (1999). This paper presents distortion functions that not only satisfy all the necessary continuity conditions, but also are valid for general quadrilateral cross sections.

After the warping and distortion functions are found, the variational principle is used to obtain a one-dimensional beam theory for the analysis of coupled deformation of torsion, warping, and

Contributed by the Applied Mechanics Division of THE AMERICAN SOCIETY OF MECHANICAL ENGINEERS for publication in the ASME JOURNAL OF APPLIED MECHANICS.
Discussion on the paper should be addressed to the Technical Editor, Professor Lewis T. Wheeler, Department of Mechanical Engineering, University of Houston, Houston, TX 77204-4792, and will be accepted until four months after final publication of the paper itself in the ASME JOURNAL OF APPLIED MECHANICS.
Manuscript received by the ASME Applied Mechanics Division, June 16, 1998; final revision, Jan. 6, 1999. Associate Technical Editor: J. N. Reddy.

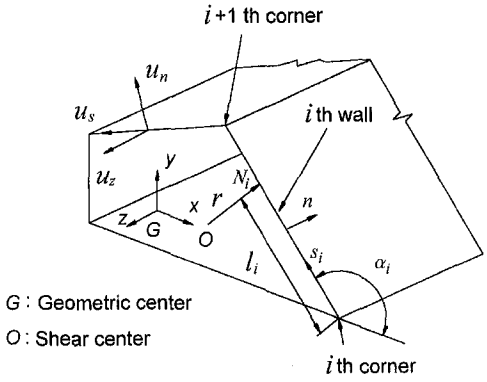

Fig. 1 Displacements at an arbitrary point on the contour of a thin-walled beam with a quadrilateral cross section

distortion. Although some closed-form solutions are possible in some special cases, we carry out numerical analysis by developing two-node C^0 finite elements. For the present finite element, only the measures of torsion, warping, and distortion are considered as the field variables. No particular effort is made in estimating the effects of the use of high-order, field-consistent, or mixed finite elements. Several numeral results by the present analysis are compared with the existing as well as the plate finite element results.

Basic Field Equation and Assumption

Figure 1 shows the contour of a thin-walled beam with a general quadrilateral cross section. The uniform contour thickness t is assumed to be much smaller than the beam length L. The contour is also assumed to be in-extensional. A right-handed curvilinear coordinate system (n, s, z) is introduced in addition to the Cartesian coordinate system (x, y, z). The tangential coordinate s is measured along the contour, and different origins are used for each wall as indicated in Fig. 1. The normal coordinate n directs outwards from the contour in the figure. The line ON_i is normal to the ith contour, where O is the shear center of the cross section and N_i is a generic point on the ith contour. The ith contour connects the ith and $(i + 1)$th corners.

It is convenient to describe the displacement of a point on the contour in terms of the normal $u_n(s, z)$, tangential $u_s(s, z)$, and axial $u_z(s, z)$ components as indicated in Fig. 1. If the beam deformation measures at given z are represented by the amounts of axial rotation $\theta(z)$, warping $U(z)$, and distortion $\chi(z)$, the shell displacements may be written as

$$u_s(s, z) = \psi_s^\theta(s)\theta(z) + \psi_s^U(s)U(z) + \psi_s^\chi(s)\chi(z) \quad (1a)$$

$$u_n(s, z) = \psi_n^\theta(s)\theta(z) + \psi_n^U(s)U(z) + \psi_n^\chi(s)\chi(z) \quad (1b)$$

$$u_z(s, z) = \psi_z^\theta(s)\theta(z) + \psi_z^U(s)U(z) + \psi_z^\chi(s)\chi(z) \quad (1c)$$

where $\psi(s)$ denote the preassigned functions of s describing the contour deformations in the n-s plane per unit value of U, θ, and χ. A major issue in the thin-walled beam analysis is how to find the correct form of $\psi(s)$, particularly the form of $\psi^\chi(s)$.

By considering the rotation $\theta(z)$ of the beam cross section about the positive z-axis, one can identify $\psi^\theta(s)$ as

$$\psi_s^\theta(s) = r(s)$$

$$\psi_n^\theta(s) = -l_i + s$$

$$\psi_z^\theta(s) = 0 \quad (2)$$

where $r(s)$ is the distance normal to the contour from the shear center O, and l_i denotes the distance from the origin of the s coordinate on the ith wall to the point N_i.

When the warping deformation $U(z)$ is considered, only the axial displacement $u_z(s, z)$ is significant so that one may assume that

$$\psi_s^U(s) = 0, \quad \psi_n^U(s) = 0, \quad \psi_z^U(s) \neq 0 \quad (3)$$

where $\psi_z^U(s)$ will be determined in the next section.

For the consideration of the in-plane distortional (or lozenging) deformation $\chi(z)$, the axial displacement can be assumed to be zero.

$$\psi_s^\chi(s) \neq 0, \quad \psi_n^\chi(s) \neq 0, \quad \psi_z^\chi(s) = 0 \quad (4)$$

The specific functional form of $\psi_s^\chi(s)$ and $\psi_n^\chi(s)$ will be investigated in the next section. As pointed out in the Introduction, one of the major contributions of this work is to determine the correct form of these functions, which is valid for general quadrilateral cross sections.

Once the shell displacements are found, three-dimensional displacements $\tilde{u}_n$, $\tilde{u}_s$, and $\tilde{u}_z$ can be found on the assumption that the beam wall thickness is much smaller than the beam length.

$$\tilde{u}_n(n, s, z) \approx u_n(s, z) = \psi_n^\theta(s)\theta(z) + \psi_n^\chi(s)\chi(z) \quad (5a)$$

$$\tilde{u}_s(n, s, z) \approx u_s(s, z) + n\frac{\partial u_n(s, z)}{\partial s}$$

$$\approx \psi_s^\theta(s)\theta(z) + \psi_s^\chi(s)\chi(z) + n\frac{d\psi_n^\chi(s)}{ds}\chi(z) \quad (5b)$$

$$\tilde{u}_z(n, s, z) \approx u_z(s, z) = \psi_z^U(s)U(z) \quad (5c)$$

Equations (5) are then used to find the following three-dimensional strain components:

$$\epsilon_{zz} = \frac{\partial \tilde{u}_z}{\partial z} = \psi_z^U(s)\frac{dU(z)}{dz} \quad (6a)$$

$$\epsilon_{zs} = \frac{1}{2}\left(\frac{\partial \tilde{u}_z}{\partial s} + \frac{\partial \tilde{u}_s}{\partial z}\right)$$

$$\approx \frac{1}{2}\left(\frac{d\psi_z^U(s)}{ds}U(z) + \psi_s^\theta(s)\frac{d\theta(z)}{dz} + \psi_s^\chi(s)\frac{d\chi(z)}{dz}\right) \quad (6b)$$

$$\epsilon_{ss} = \frac{\partial \tilde{u}_s}{\partial s} = n\frac{\partial^2 u_n}{\partial s^2} = n\frac{d^2\psi_n^\chi}{ds^2}\chi(z). \quad (6c)$$

Other strain components are negligible in comparison with these components.

Once the strain components are defined, the corresponding stresses can be easily found from the following constitutive relation:

$$\sigma_{zz} = E_1(\epsilon_{zz} + \nu\epsilon_{ss})$$

$$\sigma_{ss} = E_1(\epsilon_{ss} + \nu\epsilon_{zz})$$

$$\sigma_{sz} = 2G\epsilon_{sz} \quad (7)$$

with

$$E_1 \equiv \frac{E}{1 - \nu^2}$$

where E, G are Young's and shear moduli, respectively, and ν is Poisson's ratio. If needed, the shear stress components σ_{xz} and σ_{yz} can be computed from

$$\sigma_{xz} = \sigma_{sz}\cos\alpha_i$$

$$\sigma_{yz} = \sigma_{sz}\sin\alpha_i \quad (8)$$

where α_i is the angle between the horizontal axis (x-axis) and the tangential direction of each wall, as shown in Fig. 1. For more

detailed accounts of the basic field equations and assumptions see Vlasov (1961).

Warping and Distortion Functions

In this section, the procedure to determine the approximate form of the warping (ψ_z^U) and distortion (ψ_s^X, ψ_n^X) functions will be presented. As the underlying concept to find approximate warping and distortion functions, we propose to impose the condition such that the virtual work done by the warping and distortion stress vanishes under certain rigid-body virtual displacement fields. We denote the rigid-body virtual translations and rotations in the directions of x, y, and z by (δU_x, δU_y, δU_z) and ($\delta\Theta_x$, $\delta\Theta_y$, $\delta\Theta_z$), respectively.

1 Warping Function. The warping function is much easier to find in comparison with the distortion function. However, the understanding of this procedure is very important for the determination of the distortion function, which will be discussed shortly.

From Eqs. (6), (7), the nonzero stress components by warping, which will be superscribed by U, are given by

$$\sigma_{zz}^U(z) = E_1\psi_z^U(s)\frac{dU(z)}{dz}, \quad \sigma_{sz}^U = G\frac{d\psi_z^U}{ds}U(z). \tag{9}$$

It is noted that the warping deformations generally result from flexural and torsional deformations. This means that the following virtual work due to δU_x, δU_y, and $\delta\Theta_z$ does not generally vanish, so that no condition to determine the function ψ_z^U can be obtained from this consideration.

$$\delta W_{\text{warping}} = \int_A [r(s)\sigma_{sz}^U\delta\Theta_z + \sigma_{xz}^U\delta U_x + \sigma_{yz}^U\delta U_y]dA \tag{10}$$

However, a condition to determine the warping function can be found from the fact that no virtual work should be done by the warping stress due to the rigid-body motions associated with axial extensional and bending motions. This statement can be expressed as

$$0 = \delta W_{\text{warping}} = \int_A \sigma_{zz}^U[\delta U_z - y(s)\delta\Theta_x + x(s)\delta\Theta_y]dA \tag{11}$$

Since Eq. (11) holds for arbitrary virtual displacements δU_z, $\delta\Theta_x$, and $\delta\Theta_y$, the following conditions must be satisfied:

$$\int_A \psi_z^U dA = 0 \tag{12a}$$

$$\int_A \psi_z^U \cdot y(s)dA = 0 \tag{12b}$$

$$\int_A \psi_z^U \cdot x(s)dA = 0. \tag{12c}$$

To find a warping function satisfying Eqs. (12), one may assume further that the warping function $\psi_z^U(s)$ is a piecewise linear function of s. Thus the warping function $\psi_z^U(s)$ can be written in a finite series consisting of the so-called hat function $\psi_{zi}^U(s)$.

$$\psi_z^U(s) = \sum_{i=1}^{4} C_i\psi_{zi}^U(s) \tag{13}$$

The linearly varying hat function $\psi_{zi}^U(s)$ has a unit value at the ith corner and vanishes at all other corners. Applying the three conditions stated by Eqs. (12), the functional form of $\psi_z^U(s)$ can be determined where any one of constants C_i can be set equal to 1. The three-dimensional warping functions are shown in Fig. 2 for some beam cross sections.

The usual approach (see Gjelsvik, 1981) to find the warping function for thin-walled closed beams would yield

$$\psi_z^U(s) = \int_0^s (r - r_n)dA. \tag{14}$$

In Eq. (14), $r_n = 2A_1/\oint ds$ where A_1 and $\oint ds$ are the area enclosed by and the total length of the contour, respectively. The expression given by Eq. (14) agrees with the present result, but yields a trivial warping function in the case of a square cross section while the present analysis gives a nontrivial result even for a square cross section.

2 Distortion Functions. Now we will discuss the method to determine the distortion functions $\psi_s^X(s)$ and $\psi_n^X(s)$ analytically. To the authors' knowledge, the present method is developed here for the first time. The validity of the present distortion function will be verified in the subsequent section.

In investigating the deformation due to distortion, the underlying assumption is that each wall of the contour is in-extensional.

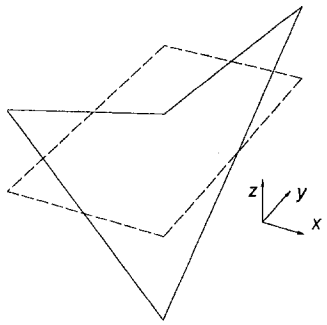

Fig. 2(*a*)

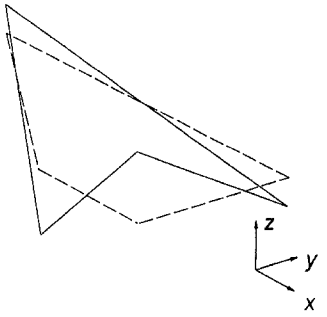

Fig. 2(*b*)

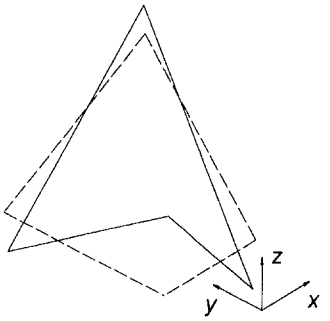

Fig. 2(*c*)

Fig. 2 Warping functions for (*a*) rectangular, (*b*) trapezoidal, and (*c*) general cross sections. (Solid lines: deformed, dotted lines: undeformed.)

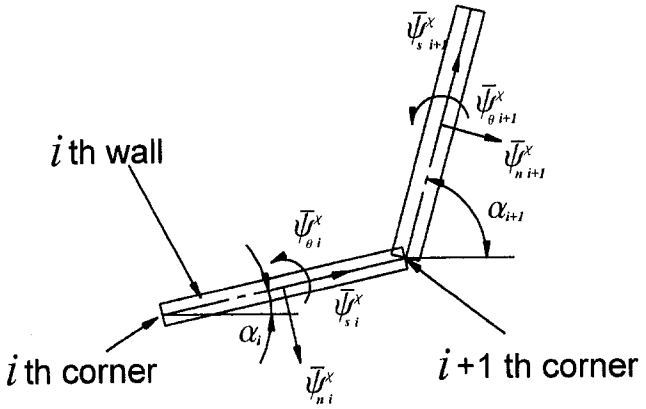

Fig. 3 Variables used to define the in-plane rigid-body deformation of the ith wall, which are associated with the contour distortion

Therefore, we first assume that each wall deforms just like a rigid body in the plane of the cross section. The amount of this deformation may be best described by the amount of rigid-body tangential ($\bar{\psi}^{\chi}_{si}$) and normal ($\bar{\psi}^{\chi}_{ni}$) translations and a rigid-body rotation ($\bar{\psi}^{\chi}_{\theta i}$) of the ith wall ($i = 1, 2, 3, 4$), measured at the center of each wall. (See Fig. 3.) In terms of these quantities, the tangential ($\psi^{\chi}_{si}(s_i)$) and normal ($\psi^{\chi}_{ni}(s_i)$) displacements in the ith wall may be expressed as

$$\psi^{\chi}_{si}(s_i) = \bar{\psi}^{\chi}_{si} \tag{15a}$$

$$\psi^{\chi}_{ni}(s_i) = \bar{\psi}^{\chi}_{ni} - (s_i - b_i/2)\bar{\psi}^{\chi}_{\theta i} \quad (0 \le s_i \le b_i,\ i = 1, 2, 3, 4) \tag{15b}$$

where b_i denotes the length of the ith wall.

The displacement continuity conditions at the corners may be expressed as

$$\psi^{\chi}_{si}|_{s_i=b_i} = \psi^{\chi}_{si+1}|_{s_{i+1}=0} \cos(\alpha_{i+1} - \alpha_i) - \psi^{\chi}_{ni+1}|_{s_{i+1}=0} \sin(\alpha_{i+1} - \alpha_i) \tag{16a}$$

$$\psi^{\chi}_{ni}|_{s_i=b_i} = \psi^{\chi}_{si+1}|_{s_{i+1}=0} \sin(\alpha_{i+1} - \alpha_i) + \psi^{\chi}_{ni+1}|_{s_{i+1}=0} \cos(\alpha_{i+1} - \alpha_i) \quad (\text{for } i = 1, 2, 3, 4;\ 5 \rightarrow 1). \tag{16b}$$

In addition to the continuity conditions expressed by Eqs. (16), the distortion displacement field must satisfy the condition similar to Eq. (11). In this case, we impose the condition that the virtual work by the distortion stress $\sigma^{\chi}_{sz}(s)$ due to the rigid-body virtual displacements δU_x, δU_y, and $\delta\Theta_z$ corresponding to flexural and torsional deformations must vanish:

$$0 = \delta W_{\text{distortion}} = \int_A [r(s)\sigma^{\chi}_{sz}\delta\Theta_z + \sigma^{\chi}_{zx}\delta U_x + \sigma^{\chi}_{zy}\delta U_y]dA. \tag{17}$$

Since $\delta\Theta_z$, δU_x, and δU_y are arbitrary, the condition stated by Eq. (17) is equivalent to the following three independent conditions:

$$\sum_{i=1}^{4} \int r(s_i)(\sigma^{\chi}_{sz})_i dA = 0 \tag{18a}$$

$$\sum_{i=1}^{4} \int (\sigma^{\chi}_{sz})_i \cos\alpha_i dA = 0 \tag{18b}$$

$$\sum_{i=1}^{4} \int (\sigma^{\chi}_{sz})_i \sin\alpha_i dA = 0 \tag{18c}$$

where subscribed quantities are associated with the ith wall. Equations (16) and (18) give 11 conditions to determine 12 unknown variables, $\bar{\psi}^{\chi}_{si}$, $\bar{\psi}^{\chi}_{ni}$, and $\bar{\psi}^{\chi}_{\theta i}$ ($i = 1, 2, 3, 4$). (Note that any one of 12 unknowns can be set arbitrary.)

It should be noted that Eqs. (15) alone represent a displacement field with rotation discontinuity at the corners; corners behave as hinges with this displacement field. Vlasov (1961) suggests a modification of the distortion function form in order to satisfy the rotation continuity. Though Vlasov's modification is useful for stress analysis, Vlasov's modified distortion function for rectangular cross sections now violates the displacement continuity at the corners. Subsequently, his approach does not seem to be proper for dynamic problems and is difficult to extend for general quadrilateral cross sections.

In what follows we propose a new method which guarantees the rotation/moment as well as the displacement continuities at the corners. In order to meet the rotation/moment continuity, the normal displacement $\psi^{\chi}_{ni}(s_i)$ is replaced by a cubic function

$$\psi^{\chi}_{ni}(s_i) = D_{i0} + D_{i1}s_i + D_{i2}s_i^2 + D_{i3}s_i^3 \tag{19}$$

while the tangential displacement $\psi^{\chi}_{si}(s_i)$ given by Eq. (15a) remains unchanged. For subsequent analysis, it is convenient to introduce new quantities $\beta_{i(i)}$ and $\beta_{i(i+1)}$, which are defined as the rotations of the ith wall at the ith and $(i + 1)$th corners.

The constants D_{i0} through D_{i3} in Eq. (19) must be selected to satisfy the following conditions:

$$\psi^{\chi}_{ni}|_{s_i=0} = \bar{\psi}^{\chi}_{ni} + \bar{\psi}^{\chi}_{\theta i}\frac{b_i}{2} \tag{20a}$$

$$\psi^{\chi}_{ni}|_{s_i=b_i} = \bar{\psi}^{\chi}_{ni} - \bar{\psi}^{\chi}_{\theta i}\frac{b_i}{2} \tag{20b}$$

$$\frac{d}{ds_i}[\psi^{\chi}_{ni}(s_i)]_{s_i=0} = \beta_{i(i)} \tag{20c}$$

$$\frac{d}{ds_i}[\psi^{\chi}_{ni}(s_i)]_{s_i=b_i} = \beta_{i(i+1)}. \tag{20d}$$

Then Eq. (19) can be written as

$$\psi^{\chi}_{ni}(s_i) = \left[-\frac{2}{b_i^2}(-\beta_{i(i)} - \bar{\psi}^{\chi}_{\theta i}) + \frac{\beta_{i(i+1)} - \beta_{i(i)}}{b_i^2}\right]s_i^3 + \left[\frac{3}{b_i}(-\beta_{i(i)} - \bar{\psi}^{\chi}_{\theta i}) - \frac{\beta_{i(i+1)} - \beta_{i(i)}}{b_i}\right]s_i^2 + \beta_{i(i)}s_i + \bar{\psi}^{\chi}_{\theta i}\frac{b_i}{2} + \bar{\psi}^{\chi}_{ni}. \tag{21}$$

The deformed contour shape determined by Eq. (21) is plotted in Fig. 4.

It should be noted that Eqs. (20a, b) are exactly the same conditions used to determine $\psi^{\chi}_{ni}(s_i)$ in Eq. (15b). Since four constants $\bar{\psi}^{\chi}_{ni}$ have already been selected to satisfy the conditions expressed by Eqs. (16) and (18), the normal displacement expressed by Eq. (21) automatically satisfies these conditions. Therefore, only the additional conditions to determine $\beta_{i(i)}$ and $\beta_{i(i+1)}$ are needed.

The equations to determine eight coefficients $\beta_{i(i)}$ and $\beta_{i(i+1)}$ are provided by the rotation and moment continuity at the corners:

$$\beta_{i(i+1)} = \beta_{i+1(i+1)} \tag{22a}$$

$$\bar{M}_{i(i+1)} = \bar{M}_{i+1(i+1)} \quad (i = 1, 2, 3, 4;\ 5 \rightarrow 1). \tag{22b}$$

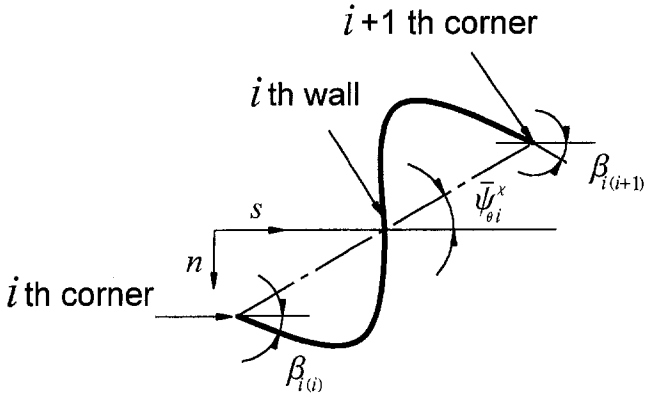

Fig. 4 A typical deformed shape of the *i*th wall of a thin-walled beam. (The displacement and rotation/moment continuities at the corner can be achieved with this distortion shape function.)

The moments $\bar{M}_{i(i)}$ and $\bar{M}_{i(i+1)}$ of the ith wall at the ith and $(i+1)$th corners are given by

$$\bar{M}_{i(i)} = M_i(s_i = 0), \quad \bar{M}_{i(i+1)} = M_i(s_i = b_i).$$

The moment $M_i(s_i)$ can be approximated by a classical beam theory:

$$M_i(s_i) = \frac{Et^3}{12}\frac{d^2\psi^{\chi}_{ni}(s_i)}{ds_i^2}$$

The corresponding bending strain through the wall thickness is given by Eq. (6*c*) where the dependence on the normal coordinate n is explicitly stated.

It is important to note again that the use of $\psi^{\chi}_{ni}(s_i)$ in Eq. (21) instead of $\psi^{\chi}_{ni}(s_i)$ in Eq. (15*b*) does not alter the displacement conditions at the corners stated by Eqs. (16) and (18). Vlasov's distortional function, valid only up to rectangular cross sections, satisfies Eqs. (22), but not (16). However, the present distortion functions $\psi^{\chi}_{ni}(s_i)$ and $\psi^{\chi}_{si}(s_i)$ satisfy all the underlying conditions. Figure 5 shows the distortion functions obtained from the present analysis for some cross sections.

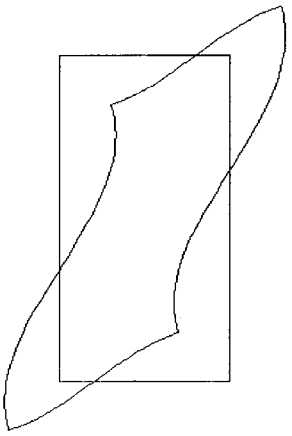

Fig. 5(*a*)

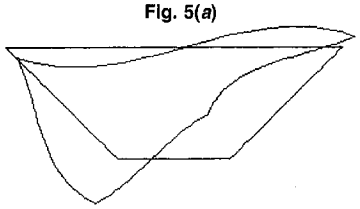

Fig. 5(*b*)

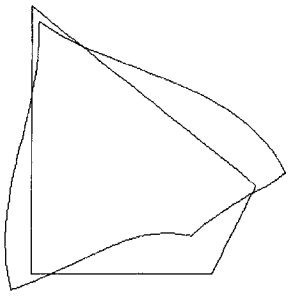

Fig. 5(*c*)

Fig. 5 Distortion functions for (*a*) rectangular, (*b*) trapezoidal, and (*c*) general cross sections

One-Dimensional Analysis

The static equilibrium equations can be obtained from the principle of the minimum potential energy (Washizu, 1982) where the potential energy Π is expressed as

$$\Pi = \tfrac{1}{2}\int \sigma_{ij}\epsilon_{ij}dV - \int (p\tilde{u}_z + q\tilde{u}_s)dV \qquad (23)$$

where p and q are the external loads in the axial and tangential directions. Substituting Eqs. (5)–(7) into Eq. (23) and integrating over the beam cross section A yields

$$\Pi = \tfrac{1}{2}\int \{aE_1U'^2 + cE_1\chi^2 + G(b_1U^2 + b_1^*\theta'^2 + b_5\chi'^2) + 2G(b_2U\theta' + b_3U\chi' + b_4\theta'\chi')\}dz - \int (p_1U + q_1\theta + q_2\chi)dz \qquad (24)$$

where $(\,)'$ denotes the differentiation with respect to z. Constants a, b_1^*, b_1, b_2, b_3, b_4, b_5 and c in Eq. (24) are

$$a = \int_A (\psi_z^U)^2 dA$$

$$b_1^* = \int_A (\psi_s^{\theta})^2 dA, \quad b_1 = \int_A \left(\frac{d\psi_z^U}{ds}\right)^2 dA$$

$$b_2 = \int_A \psi_s^{\theta}\frac{d\psi_z^U}{ds}dA, \quad b_3 = \int_A \psi_s^{\chi}\frac{d\psi_z^U}{ds}dA$$

$$b_4 = \int_A \psi_s^{\theta}\psi_s^{\chi}dA, \quad b_5 = \int_A (\psi_s^{\chi})^2 dA$$

$$c = \int_A n^2\left(\frac{d^2\psi_n^{\chi}}{ds^2}\right)^2 dA$$

and p_1, q_1, and q_2 are one dimensional load terms defined as

$$p_1 = \int_A p\psi_z^U dA; \quad q_1 = \int_A q\psi_s^{\theta}dA; \quad q_2 = \int_A q\psi_s^{\chi}dA.$$

Note that Eq. (24) is the one-dimensional version of the energy expression of Eq. (23) and constants a_1, etc., depend on the choice of $\psi^{\theta}(s)$, $\psi^U(s)$, and $\psi^{\chi}(s)$. Invoking the stationary condition on Π in Eq. (24) yields the following set of governing equations:

$$-E_1 aU'' + Gb_1 U + Gb_2\theta' + Gb_3\chi' = 0 \quad (25a)$$

$$-Gb_2 U' - Gb_1^*\theta'' - Gb_4\chi'' = 0 \quad (25b)$$

$$-Gb_3 U' - Gb_4\theta'' - Gb_5\chi'' + E_1 c\chi = 0. \quad (25c)$$

One may also identify the following generalized stress resultants H, B, and Q by examining the boundary terms appearing in the first variation of Π.

$$H \equiv \int_A \sigma_{zs}\psi_s^\theta dA = G(b_1^*\theta' + b_2 U + b_4\chi') \quad (26a)$$

$$B \equiv \int_A \sigma_{zz}\psi_z^U dA = E_1 aU' \quad (26b)$$

$$Q \equiv \int_A \sigma_{zs}\psi_s^\chi dA = G(b_5\chi' + b_3 U + b_4\theta') \quad (26c)$$

Note that these resultants H, B, and Q are the energy conjugates of Θ, U and χ, respectively.

To carry out numerical analysis, we employ a standard two-node displacement-based C^0-continuous finite element approach based on the energy form (24).[1] Following the standard procedure, the matrix equation can be obtained:

$$\mathbf{Kd} = \mathbf{P} + \mathbf{Q} \quad (27)$$

where the nodal displacement vector $\mathbf{d}$ is defined as

$$\mathbf{d} = \{\Theta_1 \quad U_1 \quad \chi_1 \quad \Theta_2 \quad U_2 \quad \chi_2\}^T. \quad (28)$$

The subscripts 1 and 2 denote the node numbers in an element level.

The load vectors $\mathbf{P}$ and $\mathbf{Q}$ are defined as

$$\mathbf{P} = \int_{-1}^{1} \mathbf{N}^T\mathbf{R}|J|d\xi \quad (29)$$

$$\mathbf{Q} = \{H_1 \quad B_1 \quad Q_1 \quad H_2 \quad B_2 \quad Q_2\}^T. \quad (30)$$

In Eq. (29), the matrix $\mathbf{N}$ is the linear shape function matrix defined as

$$\mathbf{N} = \begin{bmatrix} \frac{1}{2}(1-\xi) & 0 & 0 & \frac{1}{2}(1+\xi) & 0 & 0 \\ 0 & \frac{1}{2}(1-\xi) & 0 & 0 & \frac{1}{2}(1+\xi) & 0 \\ 0 & 0 & \frac{1}{2}(1-\xi) & 0 & 0 & \frac{1}{2}(1+\xi) \end{bmatrix} \quad (31)$$

and ξ in Eq. (29) is the dimensionless coordinate:

$$\xi = \frac{2z - (z_1 + z_2)}{z_2 - z_1} = \frac{2z - (z_1 + z_2)}{l}$$

where z_1 and z_2 are the axial coordinates of the beam elements and l is the beam element length. The Jacobian $|J|$ is simply $l/2$. The vector denoting one-dimensional load terms is defined as

$$\mathbf{R} = \{q_1 \quad p_1 \quad q_2\}^T.$$

The stiffness matrix $\mathbf{K}$ in Eq. (27) may be written explicitly as

$$\mathbf{K} = \begin{bmatrix} G\frac{b_1^*}{l} & -G\frac{b_2}{2} & G\frac{b_4}{l} & -G\frac{b_1^*}{l} & -G\frac{b_2}{2} & -G\frac{b_4}{l} \\ & E_1\frac{a}{l} + G\frac{b_1 l}{3} & -G\frac{b_3}{2} & G\frac{b_2}{2} & -E_1\frac{a}{l} + G\frac{b_1 l}{6} & G\frac{b_3}{2} \\ & & G\frac{b_5}{l} + E_1\frac{cl}{3} & -G\frac{b_4}{l} & -G\frac{b_3}{2} & -G\frac{b_5}{l} + E_1\frac{cl}{6} \\ & & & G\frac{b_1^*}{l} & G\frac{b_2}{2} & G\frac{b_4}{l} \\ & \text{—sym—} & & & E_1\frac{a}{l} + G\frac{b_1 l}{3} & G\frac{b_3}{2} \\ & & & & & G\frac{b_5}{l} + E_1\frac{cl}{3} \end{bmatrix}.$$

For dynamic analysis, Eq. (27) is replaced by

$$\mathbf{M}\frac{d^2\mathbf{d}}{dt^2} + \mathbf{Kd} = \mathbf{P} + \mathbf{Q} \quad (32)$$

where $\mathbf{d}$, $\mathbf{P}$, and $\mathbf{Q}$ are interpreted as functions of time t, and the consistent mass matrix $\mathbf{M}$ can be obtained explicitly as

$$\mathbf{M} = \rho\begin{bmatrix} (b_1^* + d_1)\frac{l}{3} & 0 & (b_4 + d_3)\frac{l}{3} & (b_1^* + d_1)\frac{l}{6} & 0 & (b_4 + d_3)\frac{l}{6} \\ & a\frac{l}{3} & 0 & 0 & a\frac{l}{6} & 0 \\ & & (b_5 + d_2)\frac{l}{3} & (b_4 + d_3)\frac{l}{6} & 0 & (b_5 + d_2)\frac{l}{6} \\ & & & (b_1^* + d_1)\frac{l}{3} & 0 & (b_4 + d_3)\frac{l}{3} \\ & \text{—sym} & & & a\frac{l}{3} & 0 \\ & & & & & (b_5 + d_2)\frac{l}{3} \end{bmatrix}$$

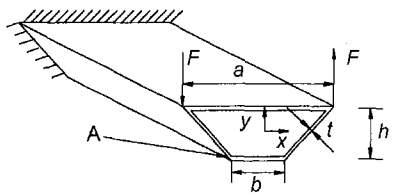

Fig. 6 Geometry of a thin-walled cantilevered beam, which may be subjected to a couple

[1] The exact solution based on the present one-dimensional theory is also given in the Appendix.

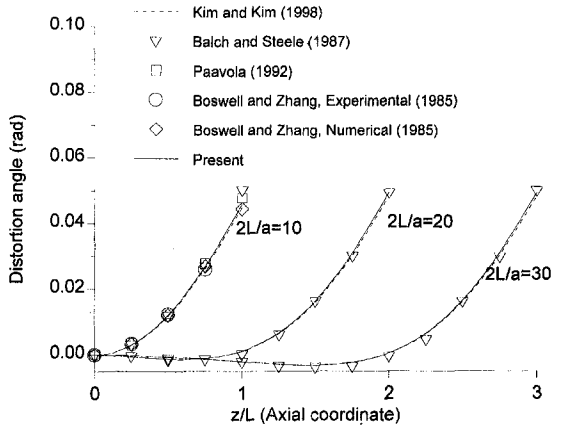

Fig. 7 Distortion of a rectangular box beam ($a = b = 300$ mm, $h = 150$ mm, $L = 1500$ mm)

where ρ is the beam density and constants d_1, d_2, and d_3 are defined as

$$d_1 = \int_A (\psi_n^\theta)^2 dA$$

$$d_2 = \int_A (\psi_n^\chi)^2 dA$$

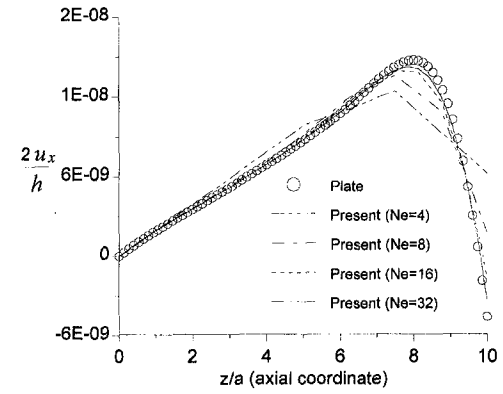

Fig. 8(*a*)

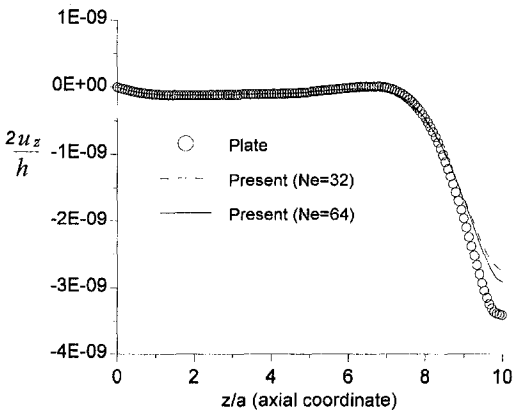

Fig. 8(*b*)

Fig. 8 The axial variation of the dimensionless displacements (*a*) $2u_x/h$, (*b*) $2u_z/h$ along corner *A* of the trapezoidal box beam subjected to a couple

Table 1 The first two eigenfrequencies for a rectangular box beam

Mode number	1	2
Method 1 (Kim and Kim; 1999)	858.69 Hz	2484.5 Hz
Method 2 (Kim and Kim; 1999)	947.39 Hz	2859.5 Hz
Present	928.95 Hz	2879.4 Hz
Plate (NASTRAN)	926.45 Hz	2836.5 Hz

$$d_3 = \int_A \psi_n^\theta \psi_n^\chi dA.$$

Once **d** is found either form Eq. (27) or Eq. (32), the stress and displacement can be calculated from the standard approach used in the finite element analysis.

Numerical Results

Example 1 *A cantilever rectangular box beam subjected to a couple.*

Before considering thin-walled beams with general quadrilateral cross sections, a rectangular box beam is first investigated to confirm the validity of the present approach. A cantilever rectangular box beam under a couple has been a subject of many earlier investigations (Boswell and Zhang, 1985; Balch and Steele, 1987; Paavola, 1992; Kim and Kim, 1999). This beam can be considered as a degenerate case with $a = b$ from the beam shown in Fig. 6 ($a = b = 300$ mm, $h = 150$ mm, $L = 1500$ mm, $t = 3.18$ mm, $E = 196.2$ kN/mm^2, $\nu = 0.27$). The magnitude of the two point loads is 4905 N, and the magnitude of the resulting torque is 1422.5 Nm (=4905 N $\times$ 290 mm). Figure 7 compares the present results for the distortional angle with the existing results; observe that the present result agrees well with the analytic solutions by Balch and Steele (1987), who employed more elaborate theories.

Example 2 *A cantilever thin-walled trapezoidal beam subjected to a couple.*

As the second example, a trapezoidal cross section ($a = 75$ mm, $b = 25$ mm, $h = 25$ mm, $t = 1$ mm, $L = 750$ mm in Fig. 6) under two point forces of unit magnitude at the free edge is considered. The material properties are $E = 200$ kN/mm^2, $\nu = 0.3$ and $\rho = 7.8 \times 10^{-6}$ kg/mm^3. The same material properties will be used in the subsequent problems. Since no published report is available for general quadrilateral cross sections, the present result will be compared with that obtained by the plate finite element analysis. Since the direct comparison for θ, χ, and U is difficult, we examine the dimensionless displacements $2u_x/h$, $2u_z/h$. Figures 8(*a, b*) indicate that the present one-dimensional result matches well with the NASTRAN (1989) *plate* finite element result.[2] As the number N_e of the present elements increases, the present results approach the plate finite element result. Somewhat slow convergence is attributed to the exponential behavior of the solution near the ends. Improved convergence may be achieved by the use of higher-order elements, but this is not the main concern of this paper.

The present exact solution for this example is also given in the Appendix, and is compared with the finite plate element result.

Example 3 *Free vibration of a free-free rectangular box beam ($a = b = 50$ mm, $h = 25$ mm, $t = 1$ mm, $L = 500$ mm).*

The advantage of the present technique is that it can be applied for both static and dynamic problems without any modification. This is due to the fact that the distortion functions ψ_n^χ and ψ_s^χ are so selected as to satisfy both the displacement and rotation (and moment) continuities at the contour corners. As a verification example of the present approach for dynamic analysis, we start with the free vibration of a thin-walled rectangular box beam with no end constraint.

Table 1 lists the first two eigenfrequencies associated with

[2] The plate results given here are converged results.

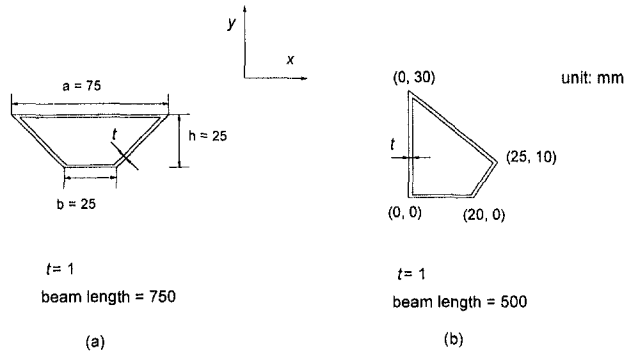

Fig. 9 The geometry of freely supported beams with (*a*) a trapezoidal and (*b*) general quadrilateral cross sections

torsion and distortion. Although not plotted here, the first vibration mode is a distortion-dominant one coupled with torsional deformation, and the second mode is a torsion-dominant mode.

In Table 1, Method 1 refers to the analysis using the same distortion function, obtained directly from Vlasov's theory, in the construction of both stiffness and mass matrices. On the other hand, Method 2 refers to the analysis using statically admissible and kinematically compatible distortion functions for the stiffness and mass matrices, respectively (see Kim and Kim, 1999). Although Method 2 yields as good results as and is simpler than the present method, Method 2 is limited only to rectangular box beams. Excellent agreement between the present and the plate finite element results is observed in Table 1.

Example 4 *Free vibration of freely supported thin-walled beams: (a) a trapezoidal cross section and (b) a general cross section.*

Now we consider the free vibration problems for (a) a trapezoidal and (b) general quadrilateral cross sections as shown in Fig. 9. The first two eigenfrequencies associated with torsional and distortional deformations are tabulated in Table 2, which compare the results from the present and NASTRAN plate finite elements. As shown in Table 2, the present analysis predicts very well the first two eigenfrequencies while the conventional theory, which considers torsion alone, cannot predict the second eigenfrequency and yields a considerably higher value for the first frequency than the present analysis.

The present first vibration mode shape for the trapezoidal box beam is reconstructed from the one-dimensional analysis, and compared in Fig. 10 with that from the plate finite element analysis. It appears from this figure that the first mode is dominated by torsional deformation. However, the effect of distortional deformation is not negligible: see Table 2.

Conclusions

New distortion shape functions are proposed for general quadrilateral cross-sectioned closed thin-walled beams. Based on these shape functions, a new one-dimensional theory dealing with coupled deformations of torsion, warping, and distortion of the thin-walled beam is presented. Several numerical results obtained by the one-dimensional finite element analysis based on the present theory have confirmed the validity of the present approach. The importance of the consideration of distortional deformation is also addressed, particularly for the dynamic analysis of thin-walled beams.

Table 2 The first two eigenfrequencies of freely supported beams in Fig. 9

Trapezoidal section shown in Fig. 9 (a)			
Mode number	Plate	Conventional beam	Present (N_e=10)
1	911.8 Hz	1258.1 Hz	909.6 Hz
2	1666.5 Hz	N/A	1696.6 Hz
General section shown in Fig. 9 (b)			
Mode number	Plate	Conventional beam	Present (N_e=10)
1	2348.3 Hz	2413.9 Hz	2335.0 Hz
2	3090.8 Hz	N/A	2951.6 Hz

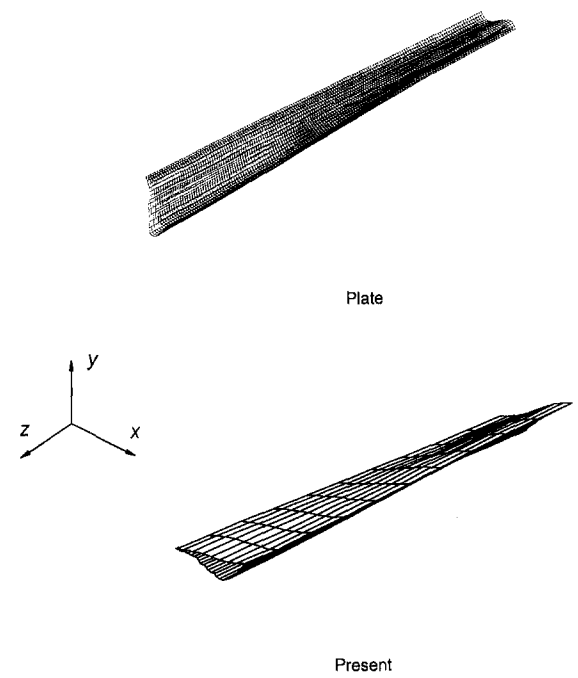

Fig. 10 The first mode of a freely supported trapezoidal box beam

Acknowledgments

The authors are grateful for the support provided by a grant from the Korea Science & Engineering Foundation (KOSEF) and Safety and Structural Integrity Research Center at the Sung Kyun Kwan University.

References

Balch, C. D., and Steele, C. R., 1987, "Asymptotic Solutions for Warping and Distortion of Thin-Walled Box Beams," ASME JOURNAL OF APPLIED MECHANICS, Vol. 54, pp. 165–173.

Bažant, Z. P., and Nimeiri, M. E., 1974, "Stiffness Method for Curved Box Girders at Initial Stress," *Journal of the Structural Division,* Vol. 100, No. ST10, pp. 2071–2090.

Bishop, R. E. D., Price, W. G., and Cheng, Z. X., 1983, "On the Structural Dynamics of a Vlasov Beam," *Proceedings of the Royal Society of London,* Vol. A388, pp. 49–73.

Boswell, L. F., and Li, Q., 1995, "Consideration of the Relationships Between Torsion, Distortion, and Warping of Thin-Walled Beams," *Thin-Walled Structures,* Vol. 21, pp. 147–161.

Boswell, L. F., and Zhang, S. H., 1983, "A Box Beam Finite Element for the Elastic Analysis of Thin-Walled Structures," *Thin-Walled Structures,* Vol. 1, pp. 353–383.

Boswell, L. F., and Zhang, S. H., 1984, "The Effect of Distortion in Thin-Walled Box-Spine Beams," *International Journal of Solids and Structures,* Vol. 20, No. 9–10, pp. 845–862.

Boswell, L. F., and Zhang, S. H., 1985, "An Experimental Investigation of the Behavior of Thin-Walled Box Beams," *Thin-Walled Structures,* Vol. 3, pp. 35–65.

Cheung, Y. K., 1969, "Folded Plate Structures by Finite Strip Method," *Journal of the Structural Division, Proceedings of ASCE,* Vol. 95, No. ST12, pp. 2963–2979.

Friberg, P. O., 1985, "Beam Element Matrices Derived From Vlasov's Theory of Open Thin-Walled Elastic Beams," *International Journal for Numerical Methods in Engineering,* Vol. 21, pp. 1205–1228.

Gere, J. M., 1954, "Torsional Vibrations of Beams of Thin-Walled Open Section," ASME JOURNAL OF APPLIED MECHANICS, pp. 381–387.

Gjelsvik, A., 1981, *The Theory of Thin Walled Bars,* John Wiley and Sons, New York.

Jirousek, J., Bougerguig, A., and Saygun, A., 1979, "A Macro-Element Analysis of Prestressed Curved Box-Girder Bridges," *Computers & Structures,* Vol. 10, pp. 467–482.

Kim, M. Y., Chang, S. P., and Kim, S. B., 1994a, "Spatial Stability and Free Vibration of Shear Flexible Thin-Walled Elastic Beams. I: Analytical Approach," *International Journal for Numerical Methods in Engineering,* Vol. 37, pp. 4097–4115.

Kim, M. Y., Chang, S. P., and Kim, S. B., 1994b, "Spatial Stability and Free Vibration of Shear Flexible Thin-Walled Elastic Beams. II: Numerical Approach,"

International Journal for Numerical Methods in Engineering, Vol. 37, pp. 4117–4140.

Kim, Y. Y., Yim, H. J., Kang, J. H., and Kim, J. H., 1995, "Reconsideration of the Joint Modelling Technique: in a Box-Beam T-Joint," SAE paper 951108, pp. 275–279.

Kim, Y. Y., and Kim, J. H., 1999, "Thin-Walled Closed Box Beam Element for Static and Dynamic Analysis," *International Journal for Numerical Methods in Engineering,* Vol. 45, pp. 473–490.

Kou, C. H., Benzley, S. E., Huang, J. Y., and Firmage, D. A., 1992, "Free Vibration Analysis of Curved Thin-Walled Girder Bridges," *Journal of Structural Engineering,* Vol. 118, No. 10, pp. 2890–2910.

Křístek, V., 1970, "Tapered Box Girders of Deformable Cross Section," *Journal of the Structural Division, ASCE,* Vol. 96, No. ST8, Proc. Paper 7489, pp. 1761–1793.

Laudiero, F., and Savoia, M., 1991, "The Shear Strain Influence on the Dynamics of Thin-Walled Beams," *Thin-Walled Structures,* Vol. 11, pp. 375–407.

Maisel, B. I., 1982, "Analysis of Concrete Box Beams Using Small-Computer Capacity," Cement and Concrete Association, Development Report 5, London.

Mikkola, M. J., and Paavola, J., 1980, "Finite Element Analysis of Box Girders," *Journal of the Structural Division, ASCE,* Vol. 106, No. ST6, pp. 1343–1357.

MSC/NASTRAN, 1989, *User's Manual,* The McNeal Schwendler Corporation, Los Angeles.

Paavola, J., 1992, "A Finite Element Technique for Thin-Walled Girders," *Computers & Structures,* Vol. 44, No. 1–2, pp. 159–175.

Razzaqpur, A. G., and Li, H. G., 1991a, "Thin-Walled Multicell Box Girder Finite Element," *Journal of Structural Engineering, ASCE,* Vol. 117, No. 10, pp. 2953–2971.

Razzaqpur, A. G., and Li, H. G., 1991b, "A Finite Element With Exact Shape Functions for Shear Lag Analysis in Multi-Cell Box-Girders," *Computers & Structures,* Vol. 39, No. 1–2, pp. 155–163.

Razzaqpur, A. G., and Li, H. G., 1994, "Refined Analysis of Curved Thin-Walled Multicell Box Girders," *Computers & Structures,* Vol. 53, No. 1, pp. 131–142.

Vlasov, V. Z., 1961, *Thin Walled Elastic Beams,* Israel Program for Scientific Translations, Jerusalem.

Washizu, K., 1982, *Variational Methods in Elasticity and Plasticity,* 3rd Ed., Pergamon Press, London.

Zhang, Z., and Chen, S., 1990, "Dynamic Finite-Element Method of Thin-Walled Beams," *AIAA Journal,* Vol. 28, No. 5, pp. 910–914.

Zhang, S. H., and Lyons, L. P. R., 1984a, "A Thin-Walled Box Beam Finite Element for Curved Bridge Analysis," *Computers & Structures,* Vol. 18, No. 6, pp. 1035–1046.

Zhang, S. H., and Lyons, L. P. R., 1984b, "The Application of the Thin-Walled Box Beam Element to Multibox Bridge Analysis," *Computer & Structures,* Vol. 18, No. 5, pp. 795–802.

APPENDIX

In order to find the closed-form solution of Eqs. (25), we introduce a function $f(z)$ such that

$$U = f'$$

$$\chi = \frac{ab_5}{cb_3} f^{(4)} - \frac{G}{E_1} \frac{b_1^*(b_1 b_5 - b_3^2) - b_2^2 b_5}{cb_3 b_1^*} f^{(2)}$$

$$\theta = \frac{-ab_5}{cb_2} f^{(4)} + \left[\frac{E_1}{G} \frac{a}{b_2} + \frac{G}{E_1} \frac{b_1^*(b_1 b_5 - b_3^2) - b_2^2 b_5}{cb_2 b_1^*} \right] f^{(2)} - \frac{b_1}{b_2} f \quad \text{(A1)}$$

where $f^{(n)}$ denotes the nth derivative of $f(z)$ with respect to z. The function f is selected to satisfy Eq. (25*a*). This approach was proposed in Vlasov (1961) for rectangular cross-sectioned beam analysis. Now the substitution of Eq. (A1) into Eq. (25*b*) or (25*c*) gives

$$f^{(6)} - 2r^2 f^{(4)} + s^4 f^{(2)} = 0 \quad \text{(A2)}$$

where

$$r^2 = \frac{1}{2} \left[\frac{b_1^*(b_1 b_5 - b_3^2) - b_2^2 b_5}{ab_5 b_1^*} \frac{G}{E_1} + \frac{c}{b_5} \frac{E_1}{G} \right]$$

$$s^4 = \frac{cb_1}{ab_5} - \frac{cb_2^2}{ab_5 b_1^*}.$$

The general solution of Eq. (A2) can be written as

$$f(z) = f_1\phi_1(z) + f_2\phi_2(z) + f_3\phi_3(z) + f_4\phi_4(z) + f_5 z + f_6 \quad \text{(A3)}$$

where f_i (i = 1, 2, 3, 4, 5, 6) are unknown coefficients to be determined from the boundary conditions. The functions ϕ_i (i = 1, 2, 3, 4) take on the following form:

$$\phi_1 = \cosh \alpha z \sin \beta z$$

$$\phi_2 = \cosh \alpha z \cos \beta z$$

$$\phi_3 = \sinh \alpha z \sin \beta z$$

$$\phi_4 = \sinh \alpha z \cos \beta z$$

where α and β are defined as

$$\alpha = \sqrt{\frac{s^2 + r^2}{2}}, \quad \beta = \sqrt{\frac{s^2 - r^2}{2}}.$$

This closed-form solution is used to solve the problem given in Example 2 and the result is compared with the finite plate element result (See Fig. A1). The present dimensionless displacement $2u_x/h$ at corner A agrees well with the finite element result, and the axial distributions of the rotation angle θ and the distortion angle γ are also plotted in Fig. A1.

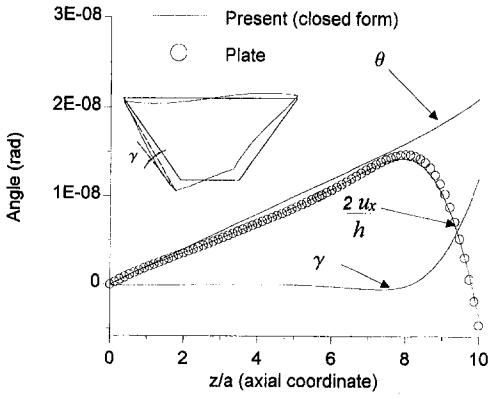

Fig. A1 The axial variation of the rotation angle θ, the distorted angle γ at an edge and the dimensionless displacement $2u_x/h$ along corner *A* of the trapezoidal box section beam subjected to a couple